Molecules and Cells

Establishment of a NanoBiT-Based Cytosolic Ca^{2+} Sensor by Optimizing Calmodulin-Binding Motif and Protein Expression Levels

Lan Phuong Nguyen[1], Huong Thi Nguyen[1], Hyo Jeong Yong[1], Arfaxad Reyes-Alcaraz[2], Yoo-Na Lee[1], Hee-Kyung Park[1], Yun Hee Na[1], Cheol Soon Lee[1], Byung-Joo Ham[3], Jae Young Seong[1], and Jong-Ik Hwang[1,*]

[1]Department of Biomedical Sciences, Korea University College of Medicine, Seoul 02841, Korea, [2]College of Pharmacy, University of Houston, Houston, TX 77204, USA, [3]Department of Psychiatry, Korea University College of Medicine, Seoul 02841, Korea
*Correspondence: hjibio@korea.ac.kr
https://doi.org/10.14348/molcells.2020.0144
www.molcells.org

Cytosolic Ca^{2+} levels ($[Ca^{2+}]_c$) change dynamically in response to inducers, repressors, and physiological conditions, and aberrant $[Ca^{2+}]_c$ concentration regulation is associated with cancer, heart failure, and diabetes. Therefore, $[Ca^{2+}]_c$ is considered as a good indicator of physiological and pathological cellular responses, and is a crucial biomarker for drug discovery. A genetically encoded calcium indicator (GECI) was recently developed to measure $[Ca^{2+}]_c$ in single cells and animal models. GECI have some advantages over chemically synthesized indicators, although they also have some drawbacks such as poor signal-to-noise ratio (SNR), low positive signal, delayed response, artifactual responses due to protein overexpression, and expensive detection equipment. Here, we developed an indicator based on interactions between Ca^{2+}-loaded calmodulin and target proteins, and generated an innovative GECI sensor using split nano-luciferase (Nluc) fragments to detect changes in $[Ca^{2+}]_c$. Stimulation-dependent luciferase activities were optimized by combining large and small subunits of Nluc binary technology (NanoBiT, LgBiT:SmBiT) fusion proteins and regulating the receptor expression levels. We constructed the binary $[Ca^{2+}]_c$ sensors using a multicistronic expression system in a single vector linked via the internal ribosome entry site (IRES), and examined the detection efficiencies. Promoter optimization studies indicated that promoter-dependent protein expression levels were crucial to optimize SNR and sensitivity. This novel $[Ca^{2+}]_c$ assay has high SNR and sensitivity, is easy to use, suitable for high-throughput assays, and may be useful to detect $[Ca^{2+}]_c$ in single cells and animal models.

Keywords: calmodulin, cytosolic Ca^{2+} sensor, internal ribosome entry site, myosin light chainC kinase 1/2, NanoBiT assay

INTRODUCTION

Intracellular cytosolic calcium (Ca^{2+}_{cyt}) is a versatile and ubiquitous second messenger in essentially all eukaryotic cells. The cytosolic Ca^{2+} concentration ($[Ca^{2+}]_c$) under resting conditions is tightly maintained around 100 nM. Cell activation by various extracellular stimulators can transiently increase $[Ca^{2+}]_c$ by up to 100-fold within a few seconds (Ma et al., 2017). Changes in $[Ca^{2+}]_c$ can be mediated by Ca^{2+} influx from the extracellular environment through ion channels, and/or by release from internal Ca^{2+} stores such as the endoplasmic reticulum (ER) (Nowycky and Thomas, 2002; Varghese et al., 2019). Transient increases in $[Ca^{2+}]_c$ are involved in regulating

Received 4 July, 2020; revised 10 September, 2020; accepted 17 September, 2020; published online 9 November, 2020

eISSN: 0219-1032

a wide array of cellular processes, including proliferation, apoptosis, fertilization, and neurotransmitter release (Varghese et al., 2019). Aberrant Ca^{2+} homeostasis has been associated with variety of diseases, including cancer, heart failure, and diabetes (Cui et al., 2017; Guerrero-Hernandez and Verkhratsky, 2014; Monteith and Bird, 2005). Therefore, $[Ca^{2+}]_c$ is considered as a good indicator of physiological and pathological cellular responses to various agents. Drug development studies utilize changes in $[Ca^{2+}]_c$ as a useful tool to screen regulators of signaling molecules that stimulate Ca^{2+} mobilization. Thus, enormous resources and efforts have been focused on developing and improving techniques to monitor changes in $[Ca^{2+}]_c$.

In general, there are two main classes of Ca^{2+}_{cyt} indicators: chemically synthesized indicators and genetically encoded calcium indicators (GECIs). Measurements of $[Ca^{2+}]_c$ became practical after the first chemical Ca^{2+}_{cyt} indicator was introduced by Roger Tsien in 1980 (Tsien, 1980). Synthetic indicators have higher signal-to-noise ratio (SNR), faster kinetics, and a larger range of $[Ca^{2+}]_c$ affinities than GECIs; however, synthetic indicators also have significant limitations. For example, synthetic dyes cannot target specific cellular organelles, and they may leak from the cell during long-term observations (Ly et al., 2020; Paredes et al., 2008). Unlike synthetic sensors, it is possible to regulate the expression levels of GECIs by incorporating the Ca^{2+}_{cyt} indicator into a plasmid with an inducible promoter. GECIs can be targeted to cell- or tissue-specific expression patterns by inserting defined signal sequences into the sensor construct (McCombs and Palmer, 2008). GECIs have been developed to measure $[Ca^{2+}]_c$ in single cells and in animal models.

Genetically encoded indicators are produced by translation of a nucleic acid sequence without the addition of any chemical compounds (Mank and Griesbeck, 2008). GECIs include fluorescent protein (FP)-based sensors detected via Förster resonance energy transfer (FRET), and bioluminescent protein (BP)-based sensors detected via a specific chemical reaction within the cell. BP-GECIs require addition of the luciferase substrate luciferin for the detection reaction, although the resulting acquired signal originates from FPs. The major drawback of FP-GECIs is that they require external illumination, which can damage cells or cause artifacts. By contrast, BP-GECIs are superior for light-sensitive applications such as optogenetics or long-term continuous monitoring (Nagai et al., 2014). Both FP-GECIs and BP-GECIs have poorer SNR than synthetic indicators (Perez Koldenkova and Nagai, 2013). A common approach to improve SNR and brightness of GECIs involves indicator overexpression driven by a strong promoter such as the cytomegalovirus (CMV), and CMV early enhancer/chicken beta actin promoter. However, under some conditions, this overexpression strategy can lead to adverse effects such as cell/tissue damage, abnormal brain activity in indicator-expressing transgenic models, nonfunctional indicators, or perturbations in membrane-gated L-type Ca^{2+} channels and distorted Ca^{2+} dynamics (Tian et al., 2009; Yang et al., 2018).

The discovery of the 19.1 kDa luciferase enzyme NanoLuc (Nluc), which is derived from the deep-sea shrimp *Oplophorus gracilirostris*, has stimulated the development of new BP-GECIs because they are 100× to 150× brighter than previous luciferase constructs (Yang et al., 2016). Nluc can be used intact or in split form consisting of Large BiT (LgBiT, 17.6 kDa) and Small BiT (SmBiT, 1.3 kDa) to study real-time protein-protein interactions based on competitive intramolecular complementation (Dixon et al., 2016). Nluc fragments are smaller than green fluorescent protein (GFP) and weakly associated, thus minimizing artifactual results in protein-protein interaction studies. Both intact and split-form Nluc can be used in intensiometric GECIs (biosensors such as the GeNL series that change fluorescence intensity when bound to an ion) or ratiometric GECIs (biosensors such as CalfluxVTN, LUCI-GECO1, and GLICO that exhibit shifts in absorption/emission spectra when bound to an ion) (Qian et al., 2019). Enormous resources have been devoted to Nluc-containing sensor design. However, most tandem sensor constructs contain FP, which might contribute to low SNR due to photobleaching or slower kinetics for large conformational changes to induce a fluorescent signal (Farhana et al., 2019). Acquisition and data manipulation for ratiometric sensors is more complicated than for intensiometric sensors due to the computation of fluorescence ratios for the former.

Specialized microscope instrumentation is required for $[Ca^{2+}]_c$ detection using intensiometric or ratiometric sensors. Ratiometric sensor monitoring of $[Ca^{2+}]_c$ change requires equipment that detects rapid changes in wavelength emission, such as confocal or two-photon microscopy, which limits their application. Chemically synthesized indicators can be detected with specialized instruments such as fluorescence imaging plate reader (FLIPR) and the FlexStation microplate reader (Luo et al., 2011; Wu et al., 2019), which are feasible for high-throughput assays for drug discovery, but expensive. Therefore, the development of a novel Ca^{2+} assay system that uses common laboratory equipment would be invaluable for applications ranging from simple signaling mechanism analysis to high-throughput drug screening.

In this study, we developed a novel intensiometric bioluminescent GECI method using split Nluc without a FP. Our calcium sensor consists of two components as fusion constructs with split Nluc fragments: calmodulin (CaM), and the calmodulin-binding peptide. We used these sensors and luminescence detection instruments to monitor real-time changes in $[Ca^{2+}]_c$ in response to extracellular stimulation. We also identified a suitable calmodulin-binding peptide and promoter to optimize expression level of the bioluminescent GECI to efficiently detect changes in $[Ca^{2+}]_c$. Although these assay data were collected from cell populations, our method may be applicable for investigating single-cell $[Ca^{2+}]_c$ responses, drug development, and *in vivo* Ca^{2+}_{cyt} imaging.

MATERIALS AND METHODS

Materials

A NanoBiT starter kit containing all plasmids and reagents for the protein interaction assay was purchased from Promega (USA). The pcDNA3.1 expression vector was purchased from Invitrogen (San Diego, CA, USA). The SRE-Luc vector containing four copies of the serum response element (SRE, CCATATTAGG) was purchased from Stratagene (USA). All

primers and reagents for gene cloning and PCR were purchased from Cosmo Genetech (Korea). DNA sequencing was conducted by Macrogen (Korea). Unless otherwise stated, all reagents were purchased from Sigma-Aldrich (USA).

Cell culture

HEK293 and HEK293T cells were obtained from the American Type Culture Collection (ATCC, USA). All cell lines in Dulbecco's modified Eagle's medium (DMEM) supplemented with 10% fetal bovine serum, 100 U/ml penicillin G, and 100 μg/ml streptomycin (Invitrogen, Carlsbad, CA, USA) were maintained at 37°C with 5% CO_2 unless otherwise stated.

Plasmid construction

Human cytomegalovirus (CMV) promoter sequence in pcDNA3.1 vector was substituted with promoter sequences of *Ubiquitin C* (UbiC), *Elongation factor* (EF), or *Herpes simplex virus thymidine kinase type 1* (HSV-tk) to develop a regulated expression system. The commercially obtained *Nano-luciferase* gene fragments in NanoBiT vectors were inserted into the multicloning site under control of each promoter sequence. The *Calmodulin* gene and calmodulin-binding region sequences in the target proteins were inserted into the vectors as N-terminal or C-terminal tags of the NanoBiT fragments. The following calmodulin-binding regions were used in these experiments: MYLK1S, MKKYMARRKWQKTGNAVRAIGRLSSMA from myosin light chain kinase 1 (MYLK1); MYLK2S, LLKKYLMKRRWKKNFIAVSAANRFKK from MYLK2; and CAMK2S, LKKFNARRKLKGAILTTMLATRNFS from Ca^{2+}-calmodulin-dependent protein kinase II (CAMK2). All *G protein-coupled receptor* (*GPCR*) genes were PCR-cloned from chromosomal DNA of HEK293 cells, and *Epidermal growth factor receptor* (*EGFR*) was obtained from Addgene (www.addgene.org/); they were inserted into the plasmid constructs by PCR and enzyme digestion. The multicistronic constructs of calmodulin-SmBiT and LgBiT-MYLK2 linked by T2A were constructed in the UbiC promoter-containing vector by PCR with appropriate primers and subsequent enzyme digestion. The internal ribosome entry site (IRES) from the pIRES vector (Takara Bio USA, USA) was inserted into the multicloning sites of vectors containing different promoters, and both NanoBiT fusion constructs (calmodulin-SmBiT and LgBiT-MYLK2S) were inserted upstream or downstream of the IRES.

NanoLuc complementation (NanoBiT) assay

HEK293 or HEK293T cells were seeded in 96-well plates at a cell density of 2×10^4 cells/well. The next day, 30 ng of receptor plasmid, 30 ng of plasmid containing calmodulin tagged with LgBiT or SmBiT, and 30 ng of plasmid containing calmodulin-binding region fused to SmBiT or LgBiT in the N-terminal or C-terminal region were mixed with 0.2 μl Lipofectamine 2000 (Invitrogen, Carlsbad, CA, USA) and added to the plated cells. Subsequent transfection steps were performed according to the manufacturer's instructions. After 24 h, media was replaced with 100 μl of Opti-MEM and cells were stabilized for 10 min at room temperature before measuring the luminescence. Then, 25 μl of Nano-Glo Live Cell Reagent (furimazine) was added to each well, and basal luminescence was measured using a luminometer (BioTek, Winooski, VT, USA) for the first 10 min. Finally, cells were stimulated by adding 10 μl of appropriate agonists to each well, and the cell plate luminescence was measured for 30 min. The schematics of all NanoBiT constructs and their combinations, and all graphs in dosing experiments were presented in supplementary information (Supplementary Figs. S1-S9). The absolute values of luciferase activities were also shown in it (Supplementary Table S1).

ERK phosphorylation

HEK293 cells in 6-well plates were transfected with 2 μg pcDNA3.1 vector harboring the receptor genes using 4 μl Lipofectamine 2000. The next day, cells were incubated with serum-free media overnight, and then treated with their cognate ligand for the indicated time. After washing with cold phosphate-buffered saline, the cells were harvested with lysis buffer (50 mM Tris-HCl pH 7.5, 150 mM NaCl, 20 mM NaF, 1% Triton X-100, and protease inhibitors) and the protein extracts were clarified by centrifugation at 15,000 rpm for 15 min at 4°C. Then, 20 μg of cellular proteins were examined using SDS-PAGE followed by western blotting with anti-pERK or anti-ERK antibodies.

Reporter gene assay

HEK293 cells were seeded in 24-well plates at a density of 8×10^4 cells/well. The next day, a mixture of 400 ng of receptor gene–containing plasmids, 50 ng of SRE-Luc reporter gene plasmids, and 1 μl of Lipofectamine 2000 was added per well according to the manufacturer's instructions. The next day, cells were maintained in serum-free DMEM overnight. Approximately 36 h after the start of transfection, cells were treated with appropriate ligands for 6 h. Cells were then lysed using 100 μl of lysis buffer, and the luciferase activity of the cell extract was measured using a luciferase assay and the standard protocol for the Synergy 2 Multi-Mode Microplate Reader (BioTek).

Statistical analysis

Statistical differences among experimental groups were analyzed by unpaired Student's *t*-tests or one-way ANOVA using Prism 5 software (GraphPad Software, USA). Group means were analyzed using Bonferroni's multiple comparison tests. Data were presented as mean ± SD, and all experiments were performed in triplicate unless otherwise indicated.

RESULTS

Screening construct combinations for the NanoBiT assay

Ca^{2+}-bound calmodulin can bind various effector molecules via distinct amino acid sequence motifs. Therefore, a structural complementation assay using NanoBiT technology must be applicable to detect $[Ca^{2+}]_c$ increases (Fig. 1A). We developed constructs containing *Calmodulin* fused to the small fragment (SmBiT) or large fragment (LgBiT) of *Nano-luciferase* at both the N-terminal and C-terminal ends using commercially obtained vectors (pNB; Promega). The calmodulin-binding motifs from MYLK1/2 (MYLK1S and MYLK2S) was inserted into four different vectors containing each of the SmBiT and LgBiT gene fragments. According to the size and position

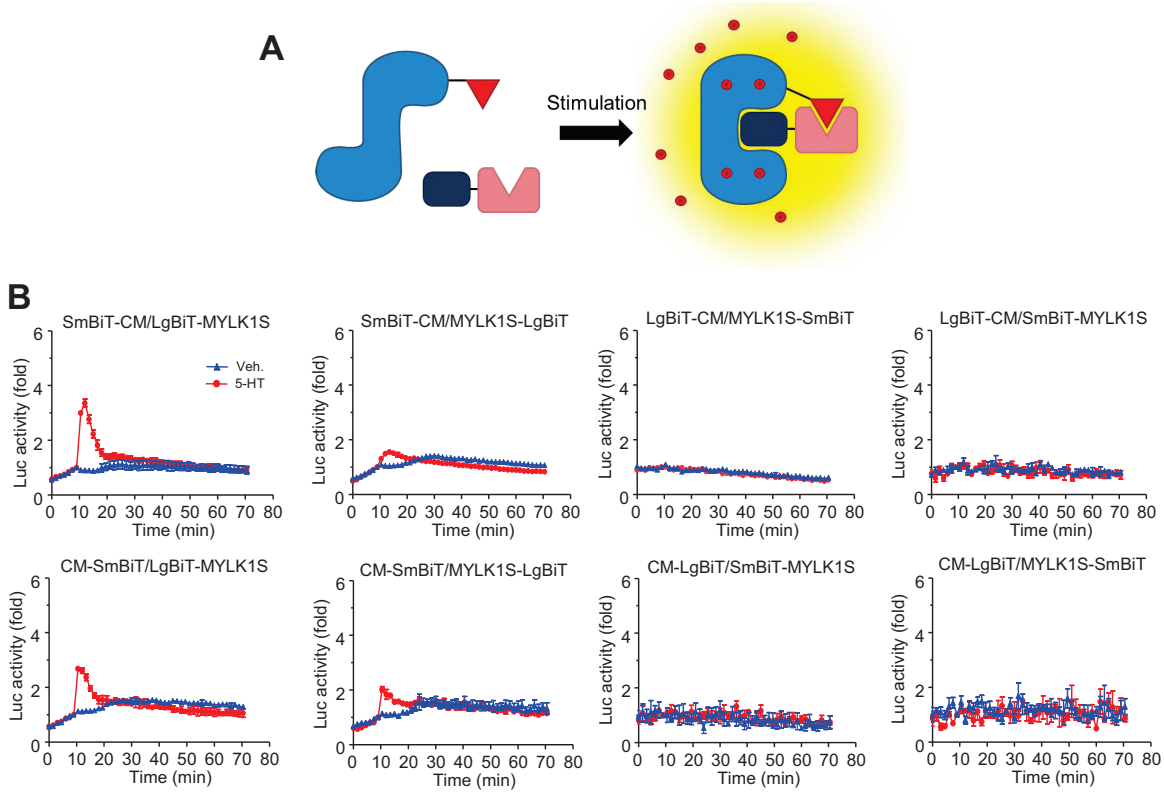

Fig. 1. NanoLuc complementation (NanoBiT) assay using calmodulin and calmodulin-binding regions. (A) Schematics of cytosolic calcium measurements with NanoBiT assay. Light blue, calmodulin; deep blue, calmodulin target region; red dots, Ca^{2+}; red triangle, SmBiT; pink, LgBiT. (B) Optimization of NanoBiT construct combinations. All eight combinations of calmodulin, the target motifs of myosin light chain kinase 1 (MYLK1S), Nluc fragments, and 5-HT2AR were expressed in HEK293T cells. 5-HT (1 μM)-induced luciferase activities were measured as described in the Materials and Methods section. CM, calmodulin; MYLK1S, calmodulin-binding region of MYLK1; Veh., vehicle. All experiments were done more than three times.

of the Nluc fragments, eight combinations of the constructs were expressed in HEK293T cells with 5-HT2AR, which stimulates intracellular calcium mobilization through the Gαq-phospholipase C pathway. Treatment of cells with 5-HT increased the luciferase activity in cells expressing combinations of SmBiT forms of calmodulin and LgBiT forms of MYLK1S (Fig. 1B).

Selecting calmodulin target motifs for efficient calcium response detection

The calmodulin-binding motifs have different amino acid sequences although they may have similar structures, suggesting that the motifs bind to calmodulin with different affinities. To identify the best calmodulin-binding motif, we further produced vector constructs expressing the NanoBiT fragments fused with the calmodulin-binding motifs of MYLK2 and CAMK2. All assays for this experiment were conducted in HEK293 cells instead of HEK293T cells to reduce receptor expression levels. All NanoBiT constructs were developed in vectors harboring the *Ubiquitin C* (UbiC) promoter instead of the original HSV-tk promoter in the commercially obtained vectors. The results showed that 5-HT stimulation of cells expressing various combinations of NanoBiT constructs increased the luciferase activities to different levels (Figs. 2A-2C). The luciferase signals of MYLK2S constructs were generally higher than those of MYLK1S and CAMK2S constructs. The combination with the highest luminescence was calmodulin-SmBiT and LgBiT-MYLK2S (third graph in Fig. 2B). The 5-HT dose-response analyses of cells expressing MYLK1S or MYLK2S constructs revealed that the saturated luciferase activities were higher in MYLK2S constructs than in MYLK1S, and the EC_{50} value of 5-HT was approximately 6-fold lower in MYLK2S than in MYLK1S (19.32 nM vs 120.6 nM, respectively) (Fig. 2D). These combined results indicate that a combination of calmodulin-SmBiT and LgBiT-MYLK2S provided the best detection of $[Ca^{2+}]_c$ increase.

Receptor-induced $[Ca^{2+}]_c$ dynamics were detected using NanoBiT constructs expressing calmodulin and MYLK2

To verify the feasibility of this $[Ca^{2+}]_c$ assay system, cells expressing calmodulin-SmBiT, LgBiT-MYLK2S, and exogenous receptors that increase $[Ca^{2+}]_c$ were treated with cognate ligands of the receptors and then subjected to the luciferase assay. Luciferase activity increased in cells expressing EGFR and GPCRs, which activate the Gαq pathway (e.g., 5-HT2AR, AGTR1, TACR1, and ADRA1A), but not in cells expressing ADRB1, which activates the Gαs pathway (Fig. 3A). These luciferase activities quickly increased in response to their cog-

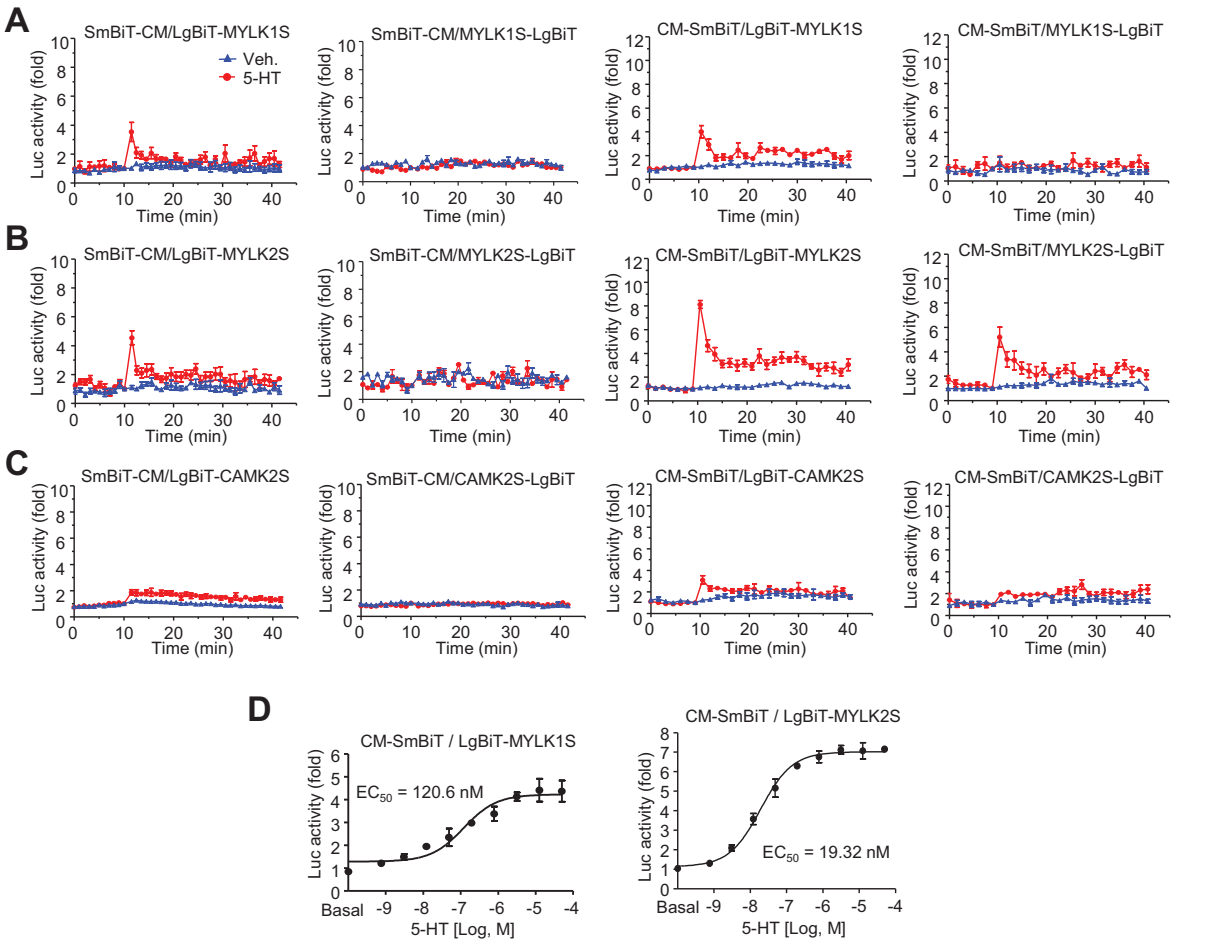

Fig. 2. Screening calmodulin-binding regions to produce efficient luciferase activities. Combinations of SmBiT-tagged calmodulin proteins at the N- or C-terminal, and LgBiT-tagged MYLK1S (A), MYLK2S (B), and CAMK2S (C) at the N- or C-terminal were coexpressed with 5-HT2AR in HEK293 cells. 5-HT-induced luciferase activities were measured as described in the Materials and Methods section. Veh., vehicle. (D) Dose dependency of 5-HT-stimulated maximum luciferase activities in cells expressing 5-HT2AR and CM-SmBiT with LgBiT-MYLK1S or LgBiT-MYLK2S. Also see Supplementary Figs. S2 and S3. Data were presented as mean ± SD. All results represent more than three different experiments.

nate ligands, but the duration of increased activity differed among the receptors. The luciferase activity peaked early and remained elevated for a long time (until 40 min, a maximum detection time) in cells expressing TACR1 and ADAR1A, whereas the activity rapidly declined in cells expressing 5-HT2AR and AGTR1.

These GPCRs also mediate ERK phosphorylation (Gooz et al., 2006; Kanazawa et al., 2015; Rhodes et al., 2009; Wu and O'Connell, 2015). When cells expressing each of the receptors were treated with its cognate ligand for different times, the duration of induced phosphorylation varied depending on the receptors. ADAR1A and TACR1-mediated phosphorylation was detected within 2 min and was sustained for 20 to 30 min. These temporal patterns were similar to the luciferase activity dynamics described above. 5-HT2AR-mediated phosphorylation was detected within 5 min and was sustained for 30 min. By contrast, AGTR1-mediated phosphorylation was detected at 10 min, indicating a slow, weak, short response (Fig. 3B). These results suggest that activation of downstream signaling molecules may depend on receptor activation intensity and individual pathway dynamics.

Enhanced $[Ca^{2+}]_c$ triggers SRE-dependent gene transcription through protein kinase C and Ca^{2+}/calmodulin-dependent kinase (CaMK) signaling pathways (Hardingham et al., 1997). ERK phosphorylation also enhances SRE-dependent transcription (Bluthgen et al., 2017; Zhang et al., 2008). We investigated correlations between SRE-dependent transcription and these signaling events (Figs. 3A and 3B) by performing reporter gene assays with cells containing each receptor and SRE-Luc. Stimulation of each receptor with the cognate ligand increased the luciferase activities to varying levels (Fig. 3C). The SRE-dependent transcriptional activities in cells expressing TACR1 and ADAR1A were high enough to reflect strong and sustained luciferase activities in NanoBiT assays and ERK phosphorylation analyses. 5-HT2AR-induced

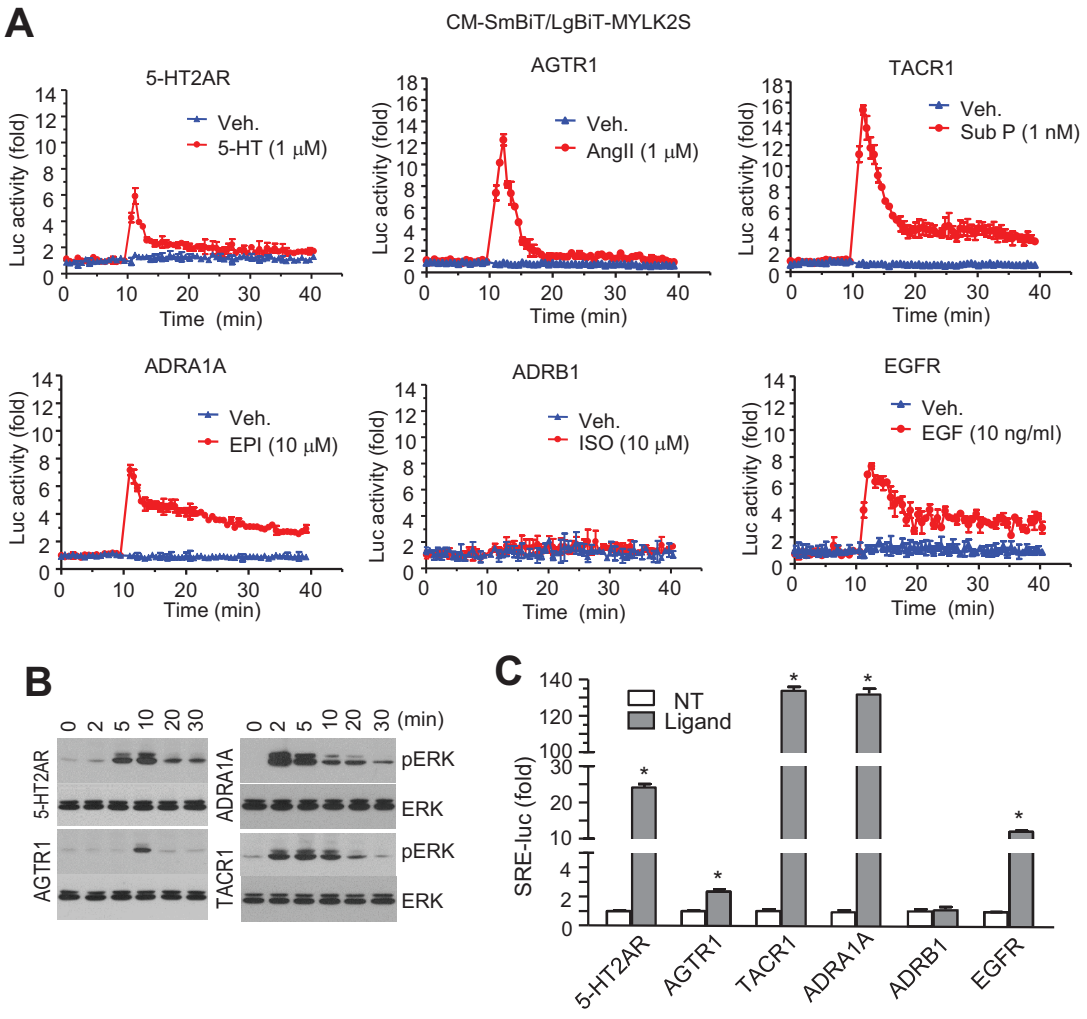

Fig. 3. Different luciferase activation patterns were observed in response to different ligands. (A) HEK293 cells expressing calmodulin-SmBiT and LgBiT-MYLK2S with various membrane receptors were treated with receptor-specific ligands, and luciferase activities were measured in real time using a luminometer. Veh., vehicle; Ang II, angiotensin II; Sub P, substance P; EPI, epinephrine; ISO, isoproterenol; EGF, epidermal growth factor. (B) ERK phosphorylation in response to receptor-specific ligands. Cells expressing the receptors were treated with their cognate ligands for the indicated times and harvested with lysis buffer. Then, 20 μg of cell extracts were analyzed with SDS-PAGE and western blotting using anti-phosphoERK or anti-ERK antibodies. (C) Cells transfected with *SRE-Luc* and each of the receptor genes were incubated with receptor-specific ligands for 6 h, and then cell lysates were analyzed for luciferase activities. $*P < 0.01$ compared to no treatment. NT, not treat. Data were presented as mean ± SD. All results represent more than three different experiments.

SRE activation appears to be predominantly mediated via the ERK pathway rather than Ca^{2+}-mediated signaling pathway. The weak AGTR1-induced SRE activation correlates with a transient decrease in $[Ca^{2+}]_c$ and ERK phosphorylation.

Optimization of receptor expression

Most assay systems that use heterologous cells expressing exogenous genes utilize CMV promoter-driven gene expression because target gene overexpression results in easily detectable cellular responses. However, the viral CMV promoter potently induces abnormally high gene expression levels, thereby precluding analyses of physiological protein function. Overexpression of G protein-coupled receptors spontaneously stimulates cellular responses without ligands (Wacker et al., 2017). Therefore, optimized expression levels of target genes may be crucial to obtain relevant output from the assay system. To optimize receptor expression levels, cells expressing receptors driven by different promoters and UbiC-driven calmodulin-SmBiT and LgBiT-MYLK2S were treated with their cognate ligands and then subjected to luciferase assay. Transcriptional potency of the promoters was determined by the GFP expression level as follows: CMV >> UbiC > HSV-tk (data not shown). Ligand-stimulated luciferase activities varied depending on the promoter. Ligand-stimulated luciferase activities of all three receptors tested were significantly higher in cells expressing UbiC-driven receptors. Receptors driven by CMV and HSV-tk promoters displayed relatively lower increases in luciferase activity (Figs. 4A and 4B). Basal luciferase ac-

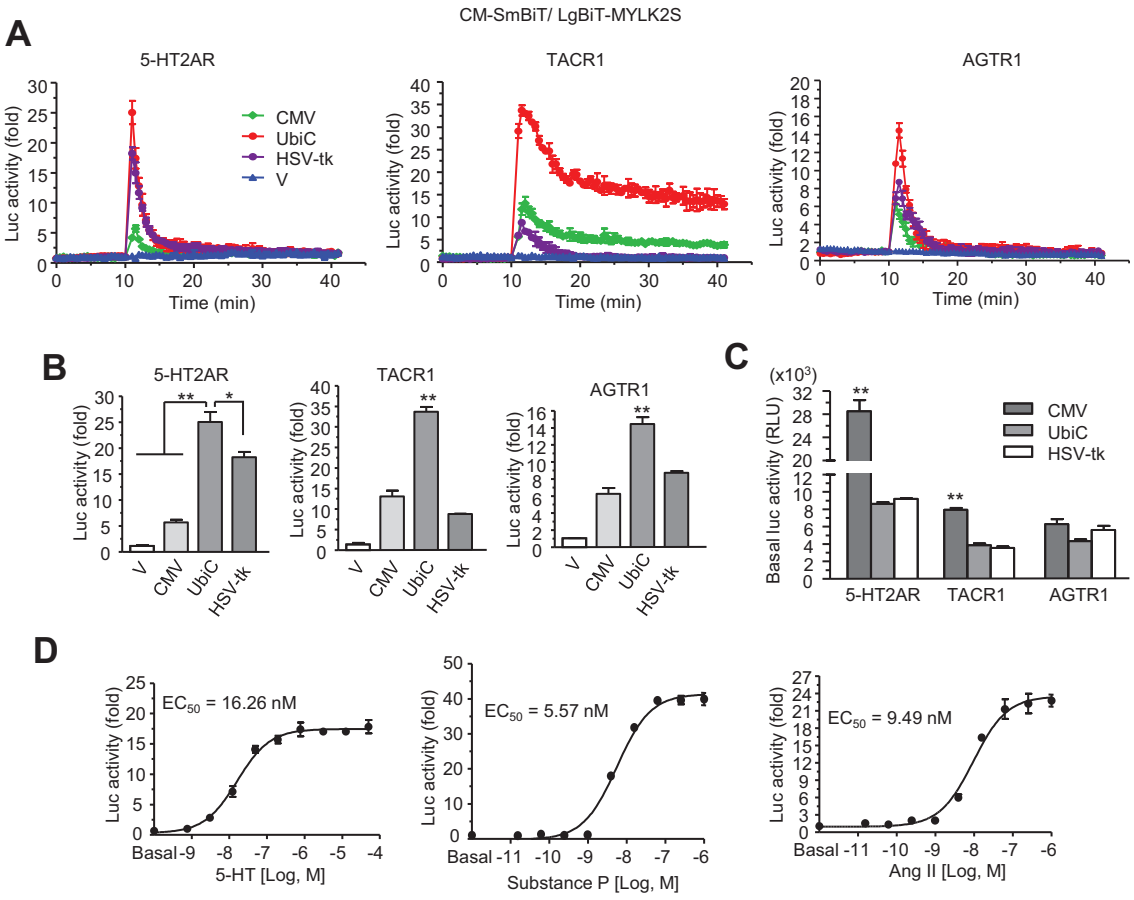

Fig. 4. Effect of receptor expression levels on ligand-induced luciferase activities. (A) Cells expressing UbiC promoter-driven CM-SmBiT and LgBiT-MYLK2S along with receptors in different promoter constructs were stimulated with ligands, and then the luciferase activities were measured. V, empty vector. (B) Comparison of the maximum ligand-induced fold-change in luciferase activity depending on receptor expression levels. Data were presented as mean ± SD. $*P < 0.01$, $**P < 0.001$ compared to other groups. (C) Basal luciferase activities among cells expressing receptors with different expression levels. Data were presented as mean ± SD. $**P < 0.001$ compared to other groups. RLU, relative light unit. (D) Dose-dependent curves of maximum ligand-induced luciferase activities in cells expressing UbiC-driven receptors. Also see Supplementary Figs. S4-S6. Data were presented as mean ± SD. All results represent more than three different experiments.

tivity levels in cells expressing receptor constructs may affect the final ligand-induced fold-increase in luciferase activity, as observed for 5-HT2AR and TACR1 (Fig. 4C). CMV-driven overexpression of 5-HT2AR and TACR1 significantly increased basal luciferase activities. By contrast, the basal activity levels were similar in HEK293 cells expressing AGTR1 under the control of three different promoters. These results suggest that receptor overexpression does not always increase basal luciferase activity. Nevertheless, UbiC-driven receptor expression is likely to produce acceptable levels of basal luciferase activity and efficient cellular responses. Finally, when cells expressing UbiC-driven receptors were treated with different amounts of the ligands, luciferase activities were increased in a dose-dependent manner with a reasonable EC_{50} value (Fig. 4D). The EC_{50} did not significantly differ between CMV-driven 5-HT2AR and UbiC-driven 5-HT2AR, but fold-increases in response to different ligand doses were easily distinguished in UbiC-driven 5-HT2AR expression.

Multigene expression system for detecting $[Ca^{2+}]_c$ dynamics

As shown above, HEK293 cell transfection efficiency is high enough to detect stimulation-dependent signaling changes even by transfection with three vectors including each of the receptor and two NanoBiT fragment constructs. However, it may be possible to reduce the number of plasmids to develop versatile applications and stable assay systems. Multicistronic expression vectors have been developed using viral gene sequences such as an IRES and a 2A self-cleavage site originated from food-and mouth disease virus (T2A). First, we developed NanoBiT constructs linked by T2A and used them for the $[Ca^{2+}]_c$ assay. The SmBiT-fused calmodulin constructs in N-ter or C-ter, which displayed relatively high ligand-induced luciferase activity, were combined with the LgBiT-MYLK2S through T2A linker under control of the UbiC promoter. The basal luciferase activities for both constructs were high compared with that of the three-vector system. The calmodulin-SmBiT construct displayed much higher basal luciferase activities than the SmBiT-Calmodulin (Fig. 5A). When

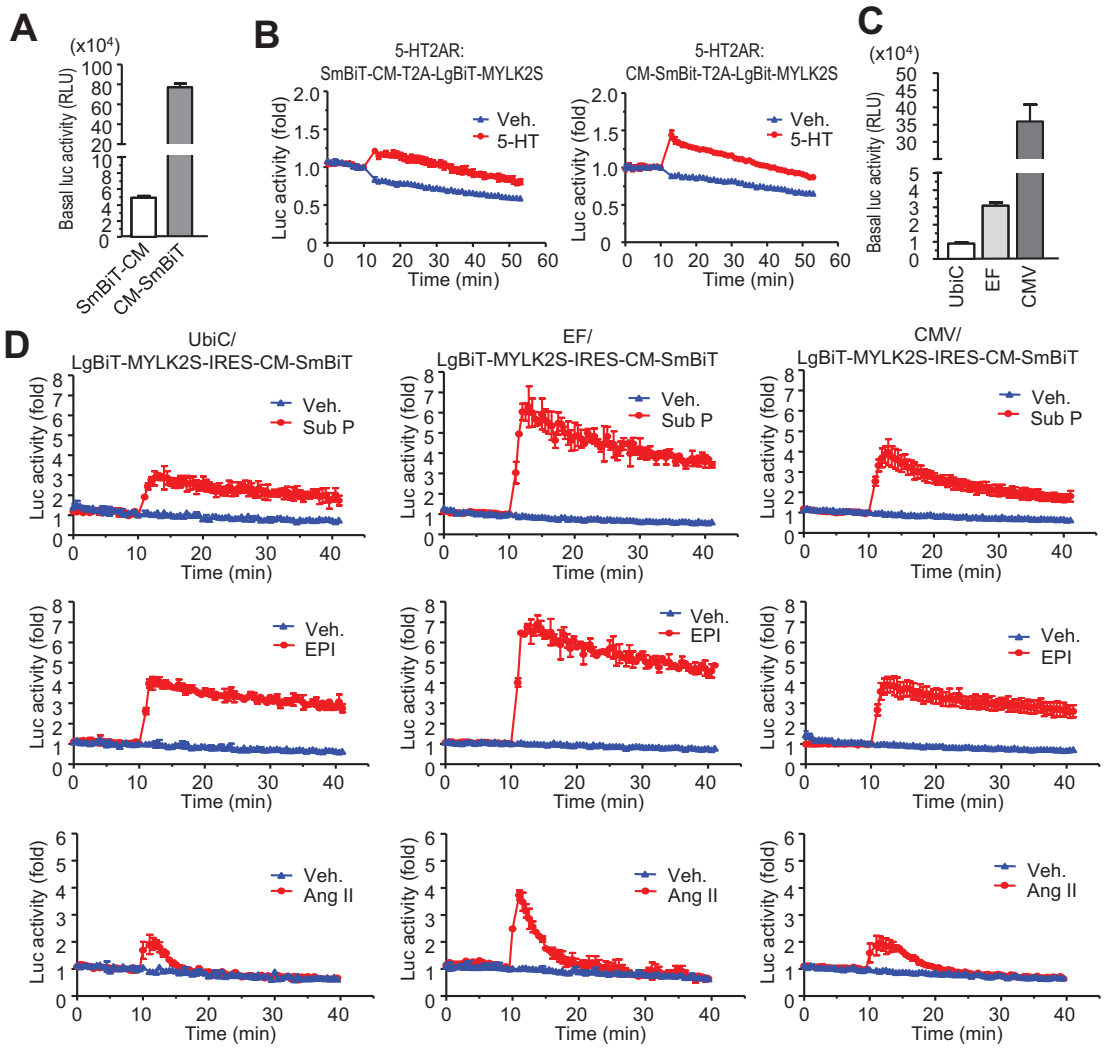

Fig. 5. NanoBiT assay using multicistronic expression vectors. (A) Different basal luciferase activities according to the calmodulin position in the T2A vector system. RLU, relative light unit. (B) Ligand-stimulated luciferase activities in cells expressing 5-HT2AR and NanoBiT constructs of calmodulin and MYLK2S in T2A vectors. Cells were treated with 5-HT and luciferase activities were measured using a luminometer. (C and D) Promoter optimization for IRES-linked NanoBiT constructs. (C) Basal luciferase activities of NanoBiT constructs of calmodulin and MYLK2S linked with IRES in vectors containing different promoters. (D) Cells transfected with different promoter-driven, IRES-linked NanoBiT constructs and UbiC-driven receptor genes were treated with ligands, and luciferase activities were measured using a luminometer. Sub P, substance P; EPI, epinephrine; Ang II, angiotensin II. Data were presented as mean ± SD. All results represent more than three different experiments.

these constructs were expressed along with 5-HT2AR, the slight fold increase of ligand-stimulated luciferase activities appeared due to higher basal luciferase activities (Fig. 5B). Next, the NanoBiT constructs were inserted into a bicistronic expression vector containing IRES. HEK293 cells transfected with the calmodulin-SmBiT-IRES-LgBiT-MYLK2S construct displayed low basal luciferase activities and poor responsiveness for ligand stimulation, which may be due to low expression of IRES-dependent LgBiT-MYLK2S. By contrast, the LgBiT-MYLK2S-IRES-calmodulin-SmBiT construct produced relatively high basal luciferase activities (data not shown). This construct was inserted into the vectors containing different promoters including UbiC, elongation factor (EF), and CMV, and then coexpressed with UbiC-driven GPCRs in HEK293 cells. The resulting basal and ligand-stimulated luciferase activities differed depending on the promoter driving the NanoBiT construct (Figs. 5C and 5D); the EF promoter resulted in the best fold-change in luciferase activity in response to all GPCR ligands compared to other promoter-driven constructs. However, these optimized fold-changes were approximately four times less than those from the three-vector system, although the temporal response patterns were similar. The high basal luciferase activities observed with the EF promoter may explain the lower stimulated fold-change (Fig. 5C), whereas the UbiC-dependent bicistronic construct likely led to very low expression of IRES-dependent calmodulin-SmBiT,

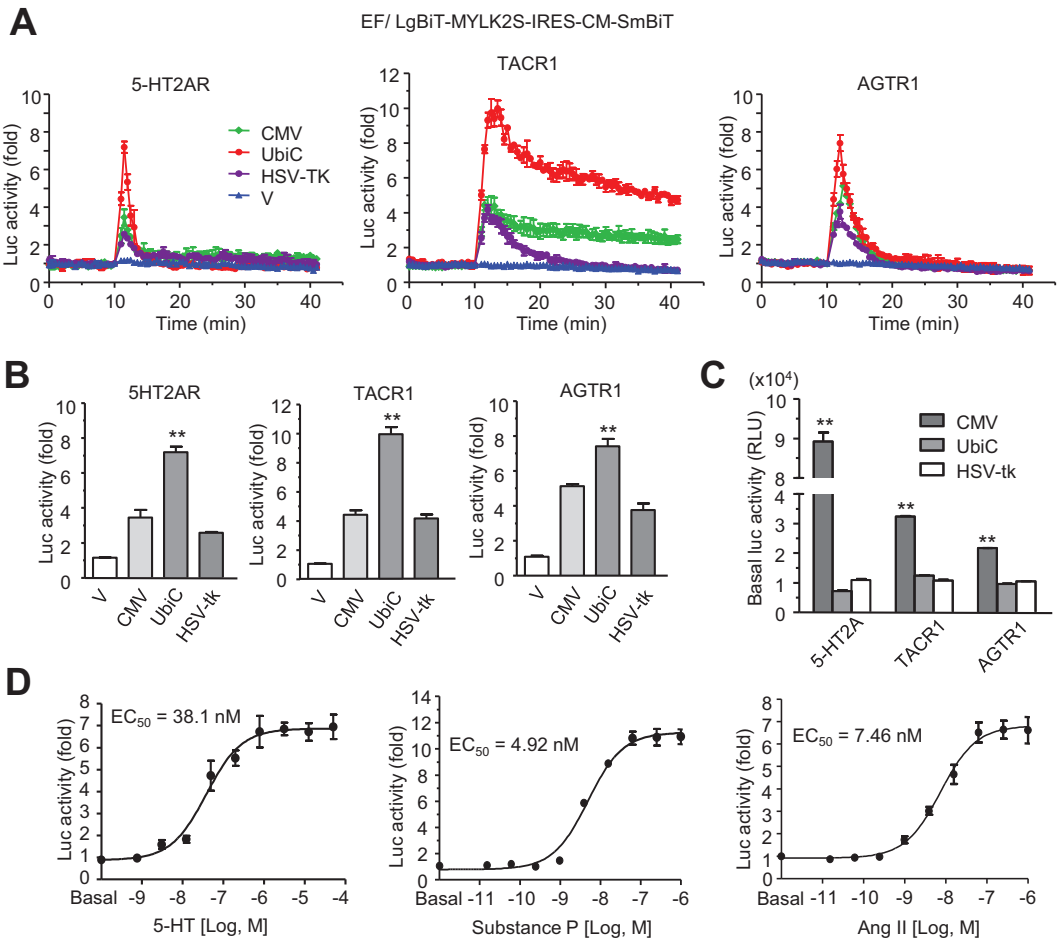

Fig. 6. Promoter optimization in receptor expression with IRES-multicistronic NanoBiT constructs. (A) Cells transfected with EF-driven LgBiT-MYLK2S-IRES-calmodulin-SmBiT and different promoter-driven receptors were treated with ligands, and luciferase activities were measured using a luminometer. V, empty vector. (B) Comparison of the maximum ligand-induced fold-change in luciferase activities depending on receptor expression levels. $**P < 0.001$ compared to other groups. (C) Basal luciferase activities depending on receptor expression level. $**P < 0.001$ compared to other groups. RLU, relative light unit. (D) Dose-dependent curves of the maximum ligand-induced luciferase activities in cells expressing UbiC-driven receptors and EF-driven, IRES-linked NanoBiT constructs (compare with Fig. 4D). Also see Supplementary Figs. S7-S9. Ang II, angiotensin II. Data were presented as mean ± SD. All results represent more than three different experiments.

which might not be sufficient to represent $[Ca^{2+}]_c$ changes. This suggests that EF-driven bicistronic NanoBiT constructs may induce suitable expression in a two-vector system.

The expression levels of all tested receptors affected ligand-induced luciferase activities in the three-vector system. To examine whether this occurs in the two-vector system, the bicistronic NanoBiT construct was expressed along with different promoter-driven GPCRs in HEK293 cells. As observed in the three-vector system, when all receptors were expressed under control of the UbiC promoter, the fold-increase in luciferase activities was much higher than those for other promoters (Figs. 6A and 6B). Basal luciferase activities in the two-vector system were much higher than those in three-vector system, as the EF promoter is stronger than the UbiC promoter (Figs. 4C and 6C). CMV-driven receptor overexpression significantly increased basal luciferase activities, which ultimately may generate a lower ligand-stimulated fold-increase in luciferase activities. When the ligand dose dependency of luciferase activities was determined in cells expressing UbiC-driven GPCRs along with the EF-driven IRES-linked NanoBiT construct, the EC_{50} values were quite similar to those from three-vector system, although their fold-increases were lower (Fig. 6D). These results suggest that the two-vector system may be useful for developing a stable Ca^{2+}_{cyt} sensor.

DISCUSSION

Bioluminescence-based Ca^{2+}_{cyt} imaging combined with FPs is potentially a useful technology for live imaging of single cells and noninvasive whole-animal imaging. The technology still has drawbacks such as low SNR, slow kinetics due to fluorescence, and potential nonspecific signals due to protein over-

expression; however, the technology does not require costly detection equipment.

In this work, we introduced a novel design for intensiometric bioluminescent GECI based on NanoBiT technology with greatly improved properties. Nluc can be split into two fragments, LgBiT and SmBiT, and subsequent interaction of their fusion proteins to acquire the enzymatic activity. Increased Ca^{2+}_{cyt} readily binds calmodulin, and the Ca^{2+}-calmodulin undergoes a conformational change to interact with target proteins through their calmodulin-binding motifs. Therefore, stimulation of cells expressing NanoBiT fusion constructs with calmodulin and calmodulin-binding motifs will increase the interactions of these constructs as $[Ca^{2+}]_c$ increases. The resulting luminescence signal decays quickly. Therefore, this protein-protein interaction (PPI)-based assay may reflect transient changes in $[Ca^{2+}]_c$ in real time. The luciferase activity resulting from construct interaction requires proper structural accessibility, and all fusion protein combinations should be tested to acquire the best sensor. The calmodulin-binding motifs must be screened to identify the one with highest affinity. We selected MYLK2S from three different motifs. Combinations that included SmBiT-fused calmodulin-binding motifs did not induce luminescence in our system. The SmBiT-fused motifs may be too small (less than 50 amino acids) to be stably expressed in cells, and the lower amount of the SmBiT constructs is not enough to detectable luciferase activities with LgBiT-fused calmodulin.

Many cell stimulators transduce signals through dynamic $[Ca^{2+}]_c$ changes; therefore a Ca^{2+}_{cyt} sensor is an excellent probe for cellular response analysis and drug development studies. Targeted GPCRs and Ca^{2+}-related ion channels can be screened and evaluated using this assay. Some GPCRs do not efficiently induce $[Ca^{2+}]_c$ increases, which restricts a universal application of this assay. This could be overcome by coexpression with Gα15/16 or utilization of Gαqi and Gαqs chimeras (Conklin et al., 1993; Zhu et al., 2008). Drug discovery studies require a rapid and simple method to efficiency test the potency of candidate compounds. We demonstrated that our $[Ca^{2+}]_c$ assay generates distinct dose-response curves for different compounds, which are easily detected using common laboratory equipment (i.e., luminometer). Our sensor also has high sensitivity and high SNR. Thus, our sensor provides a simple and robust assay for real-time monitoring of Ca^{2+}_{cyt} mobilization. We strongly believe that this system assay could be used for high-throughput assays comparing and ranking the potency of different drugs targeting the same or different receptors.

Traditionally, drug studies targeting GPCRs focused on efficacy, potency, and selectivity, whereas analysis of ligand-binding kinetics (e.g., residence time between ligand-receptor interactions) is challenging due to complex signaling transduction pathways (Hothersall et al., 2016; Strasser et al., 2017). It is becoming increasingly apparent that measuring residence time would be useful for drug development (Grundmann and Kostenis, 2017; Hothersall et al., 2016). In the current study, we used four different GPCRs (5-HT2A, AGTR1, TACR1, and ADRA1A) to evaluate the assay system kinetics in reflecting the transient $[Ca^{2+}]_c$ increases. Although these GPCRs couple to Gαq, we observed differences in peak magnitudes and signal durations. Upon stimulation, 5-HT2AR and AGTR1 induced a transient rise in $[Ca^{2+}]_c$ followed by a quick return to approximate basal, whereas TACR1 and ADRA1A peaked and then attained long-term plateaus that were much higher than basal. The differences in signal duration among the four receptors was confirmed by other assays (i.e., SRE-dependent transcription, ERK1/2 phosphorylation). These differences depend on factors such as the degree of receptor activation, inducer, and receptor preference for specific downstream responses (Charlton and Vauquelin, 2010); however, these data suggest that our Ca^{2+}_{cyt} assay could be used to examine residence time between pairs of ligand-receptor interactions. Although it remains unknown how agonist-specific properties might affect sustained cellular responses, further analysis of associations between residence time and other factors is clearly warranted.

We were not able to demonstrate comparable sensitivity between Ca^{2+}_{cyt} dynamics, SRE-dependent transcription, and ERK1/2 phosphorylation in response to receptor activation, consistent with the results of a previous study (Zhu et al., 2008). This could be explained by the versatility of GPCR-activated downstream signaling, or by the higher sensitivity of our Ca^{2+}_{cyt} assay compared to those endpoint assays including reporter gene assay and phosphorylation assay (Ma et al., 2017). Measurement of distal downstream events might enhance the SNR due to signal amplification. Thus, monitoring proximal signaling as changes in $[Ca^{2+}]_c$ seems to achieve more reliable results with minimal false positives compared to SRE-dependent transcription and ERK1/2 phosphorylation (Niedernberg et al., 2003). Our Ca^{2+}_{cyt} assay monitored Ca^{2+}_{cyt} mobilization before and after ligand addition in real time for 30 min. The ligand-stimulated changes in $[Ca^{2+}]_c$ are normalized with respect to the signal before compound addition using exactly the same sample as the background. By contrast, the endpoint assays described above measure the background signals using different samples at the same time. Taken together, we believe that our data is a more realistic reflection of receptor activation.

Although performing transient transfections is relatively simple and effortless, creating stably expressing clonal cell lines may be more suitable for high-throughput applications (Farhana et al., 2019; Wu et al., 2019). These cell lines would continuously manufacture specific indicators, thereby reducing the number of steps before the assay. However, it may be difficult to establish stable cell lines for the exogenous multigene expression system, also due to transfection efficiency. Here, we used IRES and 2A self-cleavage peptide to construct multicistronic expression vectors containing both LgBiT-MYLK2S and Calmodulin-SmBiT, which yielded promising results for establishing a stable Ca^{2+}_{cyt} sensor system. In our assay, constructs employing the T2A linker showed much higher basal luciferase activities and lower fold-increase in response to ligand stimulation. Incomplete cleavage of the T2A linker might lead to constitutive interaction of LgBiT and SmBiT. A previous study reported that tethering LgBiT and SmBiT increased their intrinsic affinity (Farhana et al., 2019), which might lead to artifactual luciferase signal. Here, we utilize IRES to separate the two proteins after translation. IRES had a critical disadvantage in that the downstream gene was trans-

lated at a much lower level than the upstream gene (Cho et al., 2017). The differences in basal luciferase activities and fold-change increases were observed when switching the positions of calmodulin-SmBiT and LgBiT-MYLK2S within the polycistronic sequence. This suggests that the calmodulin-binding motif expression level may be a critical factor to optimize the sensor, or that the separated Nluc protein constructs may undergo degradation/translocation at different rates. Further analyses of possible adverse side-effects or specific subcellular compartmentalization will be needed to establish that this is a stable and accurate Ca^{2+}_{cyt} sensor.

Although this PPI-based Ca^{2+}_{cyt} assay has advantages from both BP-GECIs and Nluc, there some potential limitations must be considered. High basal luciferase activity due to protein overexpression might hinder sensor performance, which could be observed as reduced SNR. The question is how to maintain proper basal expression levels to optimize sensor performance. The bioluminescence assay is highly sensitive, and can be affected by cell line, sensor structure, and substrate. The tested receptor expression level is often underestimated. Our data suggest that strong overexpression does not always lead to better signal output. Thus, proper receptor expression levels should be confirmed in different assay systems, including different cells and *in vivo* systems.

Usually, luciferase assays have been performed with general luminometer to measure the luciferase activity in cell population. Recent development of new equipment enables to detect the luminescence at single cell level (Yasunaga et al., 2015). Our assay method may apply to detect cytosolic Ca^{2+} change in individual cell using the equipment.

Taken together, we used NanoBiT technology to develop an innovative Ca^{2+}_{cyt} sensor with high SNR, high sensitivity, easy applicability, and suitability for high-throughput assays. GECI-mediated $[Ca^{2+}]_c$ analysis usually uses bioluminescence resonance energy transfer (BRET) technology, which requires a two-step process with bioluminescence and fluorescence. Although this achieved $[Ca^{2+}]_c$ analysis in single cells, subcellular compartments, and *in vivo* animal models, the drawbacks included low signal intensity, biased signals due to protein overexpression, and expensive detection equipment. We simplified $[Ca^{2+}]_c$ analysis using luminescence detection mediated by protein-protein interactions of Nluc fragments, which is the same concept with BRET. We examined whether the problems raised by protein overexpression (e.g., high basal activity, high SNR, biased signals) could be relieved by optimizing expression levels using different promoters. The IRES-mediated multicistronic expression system may simplify $[Ca^{2+}]_c$ analysis through promoter-mediated optimization of protein expression levels. We confirmed that each receptor mediates distinct $[Ca^{2+}]_c$ transient patterns even though they activate the same G proteins. This assay system may be useful for $[Ca^{2+}]_c$ analysis in many areas, and detect Ca^{2+}_{cyt} in single cells using specialized equipment for live-cell imaging. If the Nluc substrate can be introduced for *in vivo* imaging, our sensor assay is a promising tool to detect *in vivo* changes in Ca^{2+}_{cyt} dynamics.

Note: Supplementary information is available on the Molecules and Cells website (www.molcells.org).

ACKNOWLEDGMENTS

This work was supported by the Korea Research Foundation Grant (NRF-2019R1A2C1090051, NRF-2020M3E5D9080792) which is funded by the Ministry of Science and ICT, and partly supported by a Korea University Grant.

AUTHOR CONTRIBUTIONS

L.P.N. performed experiments and wrote the manuscript. H.T.N., H.J.Y., A.R.A., and Y.H.N. constructed plasmids. H.K.P. and Y.N.L. performed reporter gene assay. B.J.H., C.S.L., and J.Y.S. reviewed and edited the manuscript. J.I.H. supervised the experiments and wrote the manuscript.

CONFLICT OF INTEREST

The authors have no potential conflicts of interest to disclose.

ORCID

Lan Phuong Nguyen https://orcid.org/0000-0002-8932-4460
Huong Thi Nguyen https://orcid.org/0000-0002-7543-7544
Hyo Jeong Yong https://orcid.org/0000-0002-9172-3233
Arfaxad Reyes-Alcaraz https://orcid.org/0000-0002-2650-8430
Yoo-Na Lee https://orcid.org/0000-0002-9590-236X
Hee-Kyung Park https://orcid.org/0000-0001-9050-906X
Yun Hee Na https://orcid.org/0000-0002-6570-1815
Cheol Soon Lee https://orcid.org/0000-0002-7191-6791
Byung-Joo Ham https://orcid.org/0000-0002-0108-2058
Jae Young Seong https://orcid.org/0000-0002-3312-6924
Jong-Ik Hwang https://orcid.org/0000-0002-0729-1782

REFERENCES

Bluthgen, N., van Bentum, M., Merz, B., Kuhl, D., and Hermey, G. (2017). Profiling the MAPK/ERK dependent and independent activity regulated transcriptional programs in the murine hippocampus in vivo. Sci. Rep. *7*, 45101.

Charlton, S.J. and Vauquelin, G. (2010). Elusive equilibrium: the challenge of interpreting receptor pharmacology using calcium assays. Br. J. Pharmacol. *161*, 1250-1265.

Cho, J.H., Swanson, C.J., Chen, J., Li, A., Lippert, L.G., Boye, S.E., Rose, K., Sivaramakrishnan, S., Chuong, C.M., and Chow, R.H. (2017). The GCaMP-R family of genetically encoded ratiometric calcium indicators. ACS Chem. Biol. *12*, 1066-1074.

Conklin, B.R., Farfel, Z., Lustig, K.D., Julius, D., and Bourne, H.R. (1993). Substitution of three amino acids switches receptor specificity of Gq alpha to that of Gi alpha. Nature *363*, 274-276.

Cui, C., Merritt, R., Fu, L., and Pan, Z. (2017). Targeting calcium signaling in cancer therapy. Acta Pharm. Sin. B *7*, 3-17.

Dixon, A.S., Schwinn, M.K., Hall, M.P., Zimmerman, K., Otto, P., Lubben, T.H., Butler, B.L., Binkowski, B.F., Machleidt, T., Kirkland, T.A., et al. (2016). NanoLuc complementation reporter optimized for accurate measurement of protein interactions in cells. ACS Chem. Biol. *11*, 400-408.

Farhana, I., Hossain, M.N., Suzuki, K., Matsuda, T., and Nagai, T. (2019). Genetically encoded fluorescence/bioluminescence bimodal indicators for Ca(2+) imaging. ACS Sens. *4*, 1825-1834.

Gooz, M., Gooz, P., Luttrell, L.M., and Raymond, J.R. (2006). 5-HT2A receptor induces ERK phosphorylation and proliferation through ADAM-17 tumor necrosis factor-alpha-converting enzyme (TACE) activation and heparin-bound epidermal growth factor-like growth factor (HB-EGF) shedding in mesangial cells. J. Biol. Chem. *281*, 21004-21012.

Grundmann, M. and Kostenis, E. (2017). Temporal bias: time-encoded dynamic GPCR signaling. Trends Pharmacol. Sci. *38*, 1110-1124.

Guerrero-Hernandez, A. and Verkhratsky, A. (2014). Calcium signalling in diabetes. Cell Calcium *56*, 297-301.

Hardingham, G.E., Chawla, S., Johnson, C.M., and Bading, H. (1997). Distinct functions of nuclear and cytoplasmic calcium in the control of gene expression. Nature *385*, 260-265.

Hothersall, J.D., Brown, A.J., Dale, I., and Rawlins, P. (2016). Can residence time offer a useful strategy to target agonist drugs for sustained GPCR responses? Drug Discov. Today *21*, 90-96.

Kanazawa, T., Misawa, K., Misawa, Y., Uehara, T., Fukushima, H., Kusaka, G., Maruta, M., and Carey, T.E. (2015). G-protein-coupled receptors: next generation therapeutic targets in head and neck cancer? Toxins (Basel) *7*, 2959-2984.

Luo, J., Zhu, Y., Zhu, M.X., and Hu, H. (2011). Cell-based calcium assay for medium to high throughput screening of TRP channel functions using FlexStation 3. J. Vis. Exp. (54), 3149.

Ly, L.D., Ly, D.D., Nguyen, N.T., Kim, J.H., Yoo, H., Chung, J., Lee, M.S., Cha, S.K., and Park, K.S. (2020). Mitochondrial Ca(2+) uptake relieves palmitate-induced cytosolic Ca(2+) overload in MIN6 cells. Mol. Cells *43*, 66-75.

Ma, Q., Ye, L., Liu, H., Shi, Y., and Zhou, N. (2017). An overview of Ca(2+) mobilization assays in GPCR drug discovery. Expert Opin. Drug Discov. *12*, 511-523.

Mank, M. and Griesbeck, O. (2008). Genetically encoded calcium indicators. Chem. Rev. *108*, 1550-1564.

McCombs, J.E. and Palmer, A.E. (2008). Measuring calcium dynamics in living cells with genetically encodable calcium indicators. Methods *46*, 152-159.

Monteith, G.R. and Bird, G.S. (2005). Techniques: high-throughput measurement of intracellular Ca(2+) -- back to basics. Trends Pharmacol. Sci. *26*, 218-223.

Nagai, T., Horikawa, K., Saito, K., and Matsuda, T. (2014). Genetically encoded Ca(2+) indicators; expanded affinity range, color hue and compatibility with optogenetics. Front. Mol. Neurosci. *7*, 90.

Niedernberg, A., Tunaru, S., Blaukat, A., Harris, B., and Kostenis, E. (2003). Comparative analysis of functional assays for characterization of agonist ligands at G protein-coupled receptors. J. Biomol. Screen. *8*, 500-510.

Nowycky, M.C. and Thomas, A.P. (2002). Intracellular calcium signaling. J. Cell Sci. *115*, 3715-3716.

Paredes, R.M., Etzler, J.C., Watts, L.T., Zheng, W., and Lechleiter, J.D. (2008). Chemical calcium indicators. Methods *46*, 143-151.

Perez Koldenkova, V. and Nagai, T. (2013). Genetically encoded Ca(2+) indicators: properties and evaluation. Biochim. Biophys. Acta *1833*, 1787-1797.

Qian, Y., Rancic, V., Wu, J., Ballanyi, K., and Campbell, R.E. (2019). A bioluminescent Ca(2+) indicator based on a topological variant of GCaMP6s. Chembiochem *20*, 516-520.

Rhodes, D.R., Ateeq, B., Cao, Q., Tomlins, S.A., Mehra, R., Laxman, B., Kalyana-Sundaram, S., Lonigro, R.J., Helgeson, B.E., Bhojani, M.S., et al. (2009). AGTR1 overexpression defines a subset of breast cancer and confers sensitivity to losartan, an AGTR1 antagonist. Proc. Natl. Acad. Sci. U. S. A. *106*, 10284-10289.

Strasser, A., Wittmann, H.J., and Seifert, R. (2017). Binding kinetics and pathways of ligands to GPCRs. Trends Pharmacol. Sci. *38*, 717-732.

Tian, L., Hires, S.A., Mao, T., Huber, D., Chiappe, M.E., Chalasani, S.H., Petreanu, L., Akerboom, J., McKinney, S.A., Schreiter, E.R., et al. (2009). Imaging neural activity in worms, flies and mice with improved GCaMP calcium indicators. Nat. Methods *6*, 875-881.

Tsien, R.Y. (1980). New calcium indicators and buffers with high selectivity against magnesium and protons: design, synthesis, and properties of prototype structures. Biochemistry *19*, 2396-2404.

Varghese, E., Samuel, S.M., Sadiq, Z., Kubatka, P., Liskova, A., Benacka, J., Pazinka, P., Kruzliak, P., and Busselberg, D. (2019). Anti-cancer agents in proliferation and cell death: the calcium connection. Int. J. Mol. Sci. *20*, 3017.

Wacker, D., Stevens, R.C., and Roth, B.L. (2017). How ligands illuminate GPCR molecular pharmacology. Cell *170*, 414-427.

Wu, N., Nishioka, W.K., Derecki, N.C., and Maher, M.P. (2019). High-throughput-compatible assays using a genetically-encoded calcium indicator. Sci. Rep. *9*, 12692.

Wu, S.C. and O'Connell, T.D. (2015). Nuclear compartmentalization of alpha1-adrenergic receptor signaling in adult cardiac myocytes. J. Cardiovasc. Pharmacol. *65*, 91-100.

Yang, J., Cumberbatch, D., Centanni, S., Shi, S.Q., Winder, D., Webb, D., and Johnson, C.H. (2016). Coupling optogenetic stimulation with NanoLuc-based luminescence (BRET) Ca(++) sensing. Nat. Commun. *7*, 13268.

Yang, Y., Liu, N., He, Y., Liu, Y., Ge, L., Zou, L., Song, S., Xiong, W., and Liu, X. (2018). Improved calcium sensor GCaMP-X overcomes the calcium channel perturbations induced by the calmodulin in GCaMP. Nat. Commun. *9*, 1504.

Yasunaga, M., Murotomi, K., Abe, H., Yamazaki, T., Nishii, S., Ohbayashi, T., Oshimura, M., Noguchi, T., Niwa, K., Ohmiya, Y., et al. (2015). Highly sensitive luciferase reporter assay using a potent destabilization sequence of calpain 3. J. Biotechnol. *194*, 115-123.

Zhang, H.M., Li, L., Papadopoulou, N., Hodgson, G., Evans, E., Galbraith, M., Dear, M., Vougier, S., Saxton, J., and Shaw, P.E. (2008). Mitogen-induced recruitment of ERK and MSK to SRE promoter complexes by ternary complex factor Elk-1. Nucleic Acids Res. *36*, 2594-2607.

Zhu, T., Fang, L.Y., and Xie, X. (2008). Development of a universal high-throughput calcium assay for G-protein- coupled receptors with promiscuous G-protein Galpha15/16. Acta Pharmacol. Sin. *29*, 507-516.